Efficient Synthesis and Functional Replication of 3'-Deoxyapionucleic Acid (ApioNA): An RNA-Selective XNA with Conformational Flexibility

Chenghe Xiong [a #], Chunlei Zhang [b #], Lei He [a], Jun Wang [c], Yihang Gao [a], Junlin Wen [a], Congmin Liu [a], Xiaoluo Huang [a, d], You-Qiang Song [b], Yajun Wang [c*], Hui Mei [a *]

[a] Shenzhen Key Laboratory of Synthetic Genomics, Guangdong Provincial Key Laboratory of Synthetic Genomics, State Key Laboratory of Quantitative Synthetic Biology, Shenzhen Institute of Synthetic Biology, Shenzhen Institutes of Advanced Technology, Chinese Academy of Sciences, Shenzhen 518055, China

[b] Faculty of Pharmaceutical Sciences, Shenzhen University of Advanced Technology, Shenzhen 518107, China

[c] Zhejiang Cancer Hospital, The Key Laboratory of Zhejiang Province for Aptamers and Theranostics, Hangzhou Institute of Medicine (HIM), Chinese Academy of Sciences, Hangzhou 310022, China

[d] Hubei Hongshan Laboratory, Institute of Computational Synthetic Biology, College of Informatics, Huazhong Agricultural University, Wuhan 430070, China

[#] Equal contribution

* To whom correspondence should be addressed.
E-mail: hui.mei@siat.ac.cn; wangyajun@him.cas.cn

Key Words: synthetic biology, synthetic genetics, xeno-nucleic acids (XNA), artificial genetic polymers

Abstract

The development of xeno-nucleic acids (XNAs) has largely focused on two extremes: polymers that pair with both DNA and RNA, and those that avoid cross-pairing entirely. In this study, we bridge this divide by comprehensively characterizing 3'-deoxyapionucleic acid (ApioNA), which exhibits a distinct RNA-selective hybridization profile. By employing an efficient asymmetric synthesis of ApioNA building blocks, we achieved large-scale production of ApioNA oligomers and performed systematic characterization of them. Thermal melting and circular dichroism analyses reveal that ApioNA forms moderately stable duplexes with RNA but only weak duplexes with DNA and minimal self-pairing. We further establish a complete enzymatic replication cycle (DNA→ApioNA→DNA) using commercial Therminator and Bst 3.0 polymerases, achieving ~98% fidelity. Quantum mechanical calculations reveal that the apiofuranose ring adopts two low-energy puckering states, while the backbone, featuring an extra methylene group, displays enhanced conformational flexibility that favors A-form RNA geometry and requires a higher-energy state to pair with B-form DNA. This work establishes ApioNA as a practical, RNA-selective genetic polymer and demonstrates how backbone sugar chemistry can be harnessed to program the interaction specificity of synthetic genetic polymers with natural DNA and RNA.

Introduction

The pursuit of expanded chemical diversity within genetic systems is a cornerstone of modern synthetic biology.[1-3] This endeavor is driven by a dual objective: to address the limitations inherent in natural nucleic acids, and to enhance our understanding of what constitutes a genetic polymer capable of genetic information storage and transfer.[4] Xeno-nucleic acids (XNAs), which are synthetic analogs with alternative sugar or sugar-like moieties different from ribose or deoxyribose sugar found in RNA or DNA, have emerged as powerful tools to address both goals.[5] XNAs do not merely serve as synthetic constructs; they also possess tunable properties tailored to their sugar chemistry.[6] These attributes include enhanced nuclease resistance, modular hybridization specificity, and compatibility with both engineered and natural polymerases.[7] Consequently, XNAs are invaluable for a variety of applications across synthetic biology, therapeutics, and fundamental biological research.[8-9]

A central tenet of XNA research, as outlined in foundational frameworks like *The XNA Alphabet,* is that sugar chemistry serves as the primary determinant of XNA function.[6] Subtle variations in ring size, stereochemistry, or backbone linkage can dictate

hybridization behavior, enzyme recognition, and overall functionality. This understanding has led to the classification of XNAs based on their ability to interact with natural DNA and RNA, creating a functional spectrum that guides the design and application of synthetic genetic polymers.

At one end of this functional spectrum lies “compatible” XNAs—polymers that can form stable duplexes with both DNA and RNA. Examples include locked nucleic acid (LNA)[10] and 2’-fluoroarabinonucleic acid (FANA),[11] the structural proximity of which to natural nucleic acids has made them promise candidates to be used as oligonucleotide therapeutics.[12-13] A notable exception is α-L-threofuranosyl nucleic acid (TNA): a four-carbon threose based XNA whose phosphate-sugar backbone is one atom shorter than that of DNA and RNA.[14] Despite this significant structural deviation, TNA’s threose sugar adopts a C4’-exo pucker that aligns closely with the helical geometries of A-form RNA.[15] This structural compatibility enables bidirectional genetic information transfer via engineered polymerases, establishing TNA as a leading model for investigating pre-RNA genetic systems.[16] Other compatible XNAs, including hexitol nucleic acid (HNA)[17] and cyclohexenyl nucleic acid (CeNA),[18] further suggest that sugar moieties mimicking the helical parameters of natural nucleic acids normally produce polymers capable of seamless interaction with biological systems.[6]

Conversely, “orthogonal” XNAs have been designed to avoid cross-interaction with DNA and RNA, requiring specialized engineering for their function. This characteristic is crucial for applications that demand strict genetic isolation. Phosphonomethylthreosyl nucleic acid (pTNA, or tPhoNA) exemplifies this class.[19] Its sugar and backbone modifications disrupt the geometries associated with both B-form and A-form structures, which prevents stable duplex formation with DNA and RNA. Consequently, evolved polymerases, such as TgoT_EPFLH, are necessary for its enzymatic synthesis.[19] Other orthogonal systems, including pyranosyl-RNA (pRNA), xylonucleic acid (XyloNA)[20] and ZNA[21], further illustrate how sugar chemistries that diverge from conventional structural norms can give rise to polymers that function independently of natural genetic machinery.

This binary classification framework rarely accommodates XNAs displaying intermediate hybridization profiles. While 2′,5′-linked oligonucleotides—such as isoDNA and 2′,5′-RNA—exhibit preferential pairing with RNA over DNA, this selectivity originates from atypical phosphodiester connectivity rather than sugar scaffold remodeling. As such, no well-defined, sugar-modified XNA featuring robust RNA-selective binding has been reported to date.

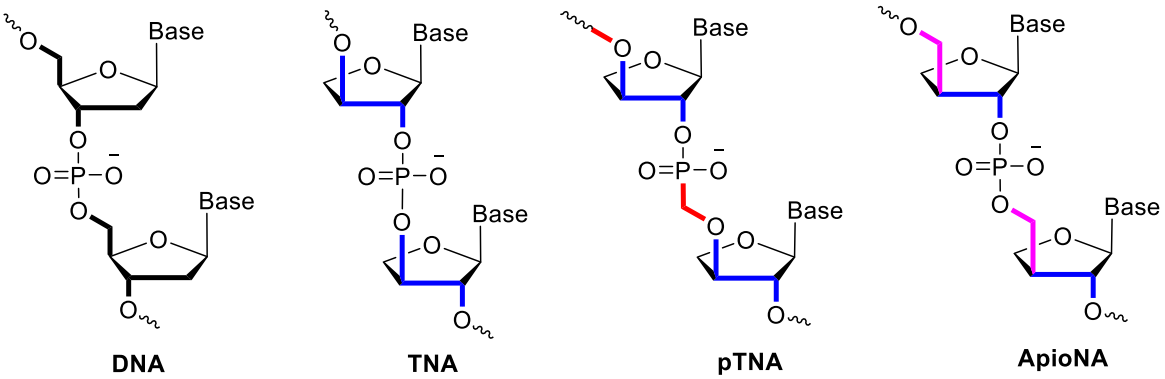

Figure 1. Constitutional structures for the linearized backbone of DNA, 3′-2′ *α*-L-threofuranosyl nucleic acid (TNA), 3′-2′ phosphonomethyl-threofuranosyl nucleic acid (pTNA) and 3′′-2′ *β*-D-3′-deoxyapiofuranosyl nucleic acid (ApioNA).

It is within this unaddressed functional gap that 3′-deoxyapionucleic acid (ApioNA) emerges as a compelling research target.[22] Though structurally homologous to TNA, ApioNA bears an additional methylene substituent at the 3′ position, which confers enhanced backbone flexibility. Distinct from pTNA's phosphonate linkage and altered CH_2/O spatial arrangement, ApioNA preserves canonical phosphodiester bonds, adopts the TNA-type 3′→2′ internucleotide connectivity, and possesses a six-atom repeating unit matching that of native DNA (Figure 1). This distinctive set of structural traits poses a core mechanistic question: does ApioNA operate as a fully compatible XNA akin to TNA, an orthogonal system analogous to pTNA, or adopt an unprecedented RNA-selective functional phenotype?

Here, we systematically characterize ApioNA and validate its distinct RNA-selective hybridization phenotype. To this end, we first developed an efficient asymmetric synthetic pathway for apioNTPs and phosphoramidites, permitting scalable production of ApioNA oligonucleotides through both solid-phase chemical synthesis and enzymatic polymerization. We demonstrate that Family B Therminator and Family A Bst 3.0 polymerases mediate a complete DNA→ApioNA→DNA replication cycle with ~98% replication fidelity. Thermal melting and circular dichroism spectroscopy further delineate ApioNA's unique duplex-forming properties: it barely forms homoduplexes, engages in weak heteroduplex formation with DNA, yet assembles moderately stable duplexes with complementary RNA. Quantum mechanical calculations further reveal the structural basis of this binding preference, showing that the apiofuranose ring adopts two low-energy puckering states and the backbone exhibits enhanced flexibility conferred by the extra methylene group. Collectively, this study establishes ApioNA as a new class of synthetic

XNAs and illustrates how sugar moiety chemistry modulates nucleic acid function, advancing our knowledge of the XNA functional landscape.

Results

1. Synthesis

The early synthesis route of 3'-deoxyapionucleoside and corresponding 3'-triphosphates (apioNTPs) involved numerous steps (≥16 steps for nucleosides, ≥23 steps for triphosphates) (**Scheme S1**) [23], leading to the insufficient yield of the sugar donor for the subsequent nucleoside preparation. Consequently, it was challenging to generate monomeric building blocks in sufficient scale for the synthesis of ApioNA oligos, and hindering studies regarding enzymatic replication or transliteration. Later, Calenbergh et al. developed a route for synthesizing 3'-deoxyapionucleoside starting from L-ascorbic acid (**Scheme S2**)[24]. However, this method also appeared unsuitable for large-scale preparation of phosphoramidites, which are normally in greater demand for the scalable solid-phase synthesis of apioNA oligos. Recently, Manoharan and colleagues reported an optimized synthetic route toward the deoxyapiose sugar donor derived from D-(+)-xylose, alongside a multi-step solid-phase strategy to access the matching apioNTPs. Even so, the preparation of both glycosyl donors and apioNTPs remains laborious and delivers low cumulative yields, limiting scalable monomer production.[25]

We recently reported an asymmetric aldol-based route to the chiral 3'-deoxyapiose backbone, initially applied only to thymidine.[26] Here, we expand this strategy to all four nucleobase phosphoramidites (A, T, C, G) through a few modifications, notably bypassing the Mitsunobu reaction. While the Mitsunobu protocol is known for its efficiency, it suffers from poor atom economy, produces stoichiometric byproducts that are difficult to remove (such as triphenylphosphine oxide and hydrazine derivatives), and relies on thermally unstable azo reagents.[27-28] By avoiding these drawbacks, our optimized approach enhances practical safety and synthetic efficiency while maintaining high stereocontrol over the 3'-deoxyapiose backbone.

This approach commenced with a one-pot cross-aldol reaction between aldehyde **1** and ethyl glyoxylate (**2**), employing diphenylprolinol as the catalyst under conditions previously reported by Hayashi.[29] The proline-mediated intermolecular aldol reaction, followed by sodium borohydride reduction, afforded a 6:1 mixture of diastereoisomers **3** with an overall yield of 60%. However, these diastereomers could not be separated by silica gel column chromatography. Alternatively, selective protection of the primary alcohol in **3** yielded the TBS ether **4** in 80% yield; subsequent debenzylation and intramolecular

lactonization produced 3-deoxyapionolactone **5** and its diastereomer **5a**, which were readily separable by silica gel column chromatography to afford the individual monomers in a combined yield of 71%. Benzoylation of **5** provided intermediate lactone **6**, which was converted to the corresponding lactol upon DIBAL-H reduction, then followed by acetylation at the anomeric position, the 3-deoxyapio glycosyl donor **7** was smoothly obtained. After several purification steps, this glycosyl donor was isolated with an overall yield of 25%.

Subsequently, nucleosides **8 (a-d)** were synthesized in a two-step process. Initially, silylated versions of nucleobases were attached to the glycosyl donor **7** through a Vorbrüggen glycosylation reaction using TMSOTf and desilylation with $Et_3N{\bullet}3HF$.[30-31] The resulting 3-deoxyapionucleosides **8 (a-d)** were obtained with 58-82% yields after purification. On one hand, global deprotection of **8 (a-d)** furnished the free nucleosides **9 (a-d)** with high yields up to 88-93%. These were then converted into the corresponding apionucleoside triphosphates (apioNTPs) **10 (a-d)** following a standard phosphorylation protocol developed by Yoshikawa and Ludwig.[32-34] The final ApioNA triphosphates were isolated as triethylammonium salts via RP-HPLC purification and lyophilization, with spectroscopic data confirming their chemical identities.

On the other hand, nucleosides **8 (a-c)** were further elaborated into advanced intermediates **11 (a-c)** through consecutive steps of 5′-OH protection with DMTrCl and selective 2′-*O*-benzoyl deprotection under mild basic conditions. This strategy preserved the acyl-protected exocyclic amines on cytosine and adenine, yielding **11 (a-c)** in 72–89% overall yield. However, after protecting the 5′-OH of nucleoside 8d with DMTrCl, subsequent hydrolysis of the 2′-O-Bz group resulted in partial cleavage of the DPC protecting group on guanine, leading to mixtures. This side reaction significantly hindered the purification of the target guanine phosphoramidite and ultimately compromising yield. To circumvent this, intermediate **8d** (after 5′-OH DMTr protection) was subjected to comprehensive deacylation, removing all acyl groups from both the sugar and base, followed by in situ protection of 2-exocyclic amino group using DMF-DMA (*N,N*-dimethylformamide dimethyl acetal),[35] affording **11d** with no need for intermediate purification. Finally, phosphitylation of the 2′-OH group in **11 (a–d)** with 2-cyanoethyl *N,N*-diisopropylchlorophosphoramidite in the presence of DIPEA generated the ApioNA phosphoramidites **12 (a–d)** in excellent yields of 75-91%. These building blocks demonstrated full compatibility with standard solid-phase DNA synthesis for the preparation of both ApioNA-containing chimeric and full ApioNA oligonucleotides (**Table**

S1).

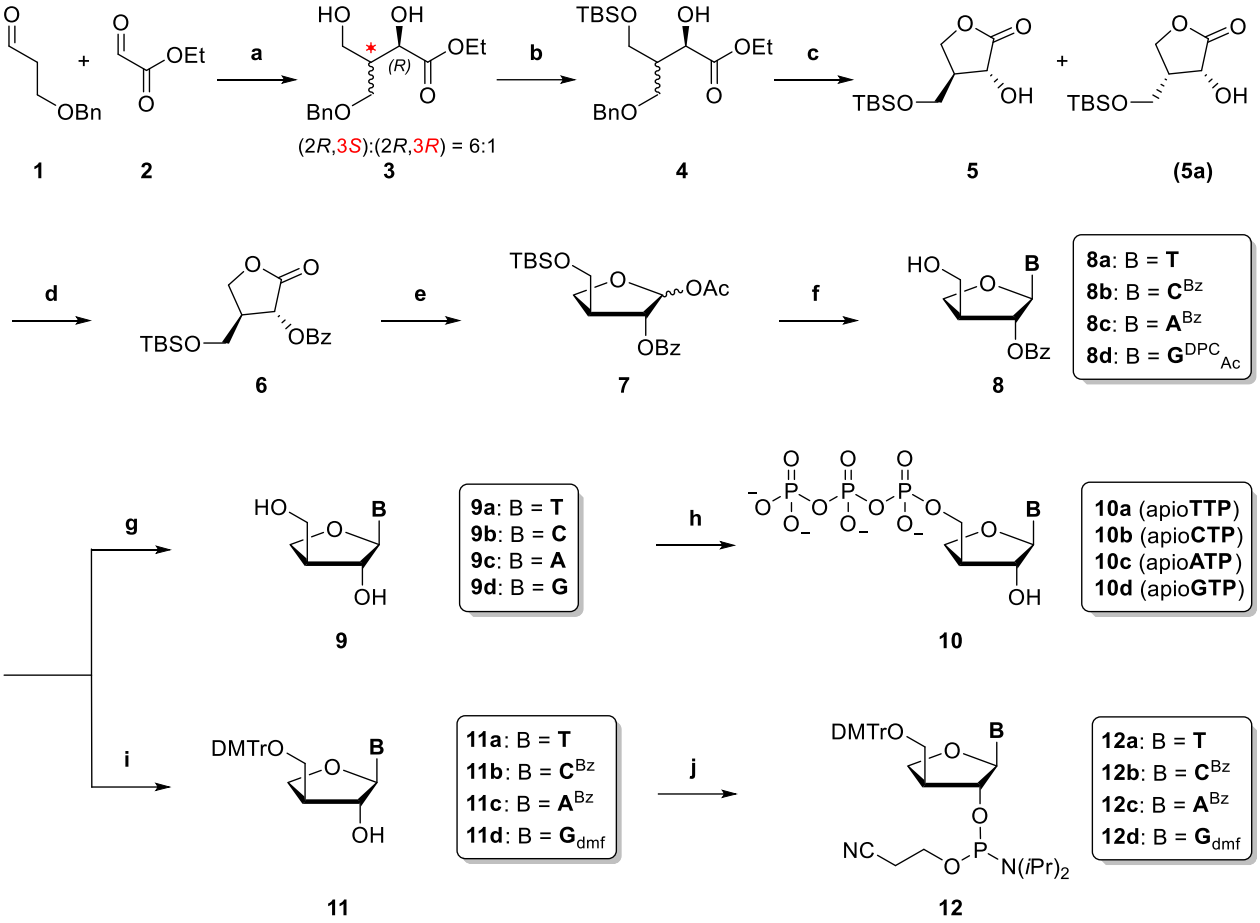

Scheme 1. Synthesis of 3'-deoxyapionucleoside triphosphates (apioNTPs) and phosphoramidites.

Reagents and conditions: (a) i. (2*S*)-*α,α*-Bis[3,5-bis(trifluoromethyl)phenyl]-2-pyrrolidinemethanol, CH_3CN-H_2O, 5 °C, 60 h; ii. $NaBH_4$, MeOH, 0°C, 30 min, 60% for two steps; (b) TBSCl, DMAP, Et_3N, CH_2Cl_2, rt, overnight, 80%; (c) i. H_2, $Pd(OH)_2$, THF, rt, 48 h; ii. 10 % mol *p*-TsOH, rt, overnight, 71% for two steps (60% for **5**, 11% for **5a**); (d) BzCl, Et_3N, CH_2Cl_2, rt, 3 h, 94%; (e) i. DIBAL-H, THF, -78 °C, 10 h; ii. Ac_2O, DMAP, Et_3N, CH_2Cl_2, 0 °C to rt, 4 h, 94% for two steps; (f) i. (for **8a**) thymine, BSA, TMSOTf, CH_3CN, rt, 2 h; (for **8b**) N^4-benzoylcytosine, BSA, TMSOTf, CH_3CN, rt, 2 h; (for **8c**) N^6-benzoyladenine, BSA, TMSOTf, toluene, 95 °C, 2.5 h; (for **8d**) N^2-acetyl-O^6-diphenylcarbamoylguanine, BSA, 1,2-dichloroethane, 70 °C, 30 min, and then TMSOTf, toluene, 70 °C, 1.5 h; ii. Et_3N•3HF, THF, overnight, rt, 82% for **8a**, 73% for **8b**, 58% for **8c**, 77% for **8d**; (g) 7 N NH_3-MeOH, overnight, rt to 60 °C, 92% for **9a**, 89% for **9b**, 88% for **9c**, 93% for **9d**; (h) i. $POCl_3$, $PO(OMe)_3$, 0 °C, 2 h; ii. tributylammonium pyrophosphate, Bu_3N, DMF, 0 °C to rt, 30 min; iii. 2 M TEAB buffer, 70% for **10a**, 62% for **10b**, 64% for **10c**, 58% for **10d**. (**i**) i. DMTrCl, pyridine, rt, 1 h; ii. (for **11a**) 7 N NH_3-MeOH, overnight, rt; (for **11b** and **11c**) 1 N NaOH, THF-MeOH, 0 °C, 25 min; (for **11d**) 7 N NH_3-MeOH, 60 °C, overnight, and then DMF-DMA, DMF, rt, overnight, 89% for **11a**, 75% for **11b**, 72% for **11c**, 82% for **11d**; (**j**) 2-cyanoethyl *N*,*N*-diisopropylchlorophosphoramidite, DIPAE, CH_2Cl_2, rt, 1 h, 91% for **12a**, 75% for **12b**, 82% for **12c**, 85% for **12d**.

2. Enzymatic Synthesis of ApioNA from Synthesized ApioNTPs

With a scalable synthetic route to all four apioNTPs established, we next explored enzymatic polymerization of these monomers on DNA templates. Prior work by Matsuda and co-workers demonstrated primer extension to generate short ApioNA products using Therminator DNA polymerase, yet further exploration was restricted by limited apioNTP availability. Enabled by our full set of synthetic apioNTPs, we herein extend this characterization to comprehensive enzymatic assays. We systematically evaluated commercial DNA polymerases for their capacity to support efficient synthesis of long-chain ApioNA (DNA → ApioNA, up to 80 nt) and the corresponding reverse transcription back to DNA (ApioNA → DNA), enabling a complete closed replication cycle. Replication fidelity was quantified using established assays previously validated for other XNA systems.[36- 37] We further assessed whether ApioNA templates can be recognized and accurately transliterated by native polymerases in *E. coli*.

2.1 Primer Extension by Commercial Polymerases for ApioNA Synthesis

We screened a panel of commercially available DNA polymerases for their ability to polymerize ApioNA from a DNA template, using a 5′-FAM-labeled 18-mer primer annealed to a 38-mer template under standardized reaction conditions (0.2 μM enzyme, 1.25 mM Mn^{2+}, 37 °C).[22, 38] Among the polymerases tested, Therminator produced the full-length product as the dominant species. Most other polymerases exhibited limited or no elongation activity (Figure **S1**). KOD XL and DeepVent™ (exo^-) stalled approximately two-thirds through the template. ApexHF, Pro Taq, and Exp Taq incorporated only 3-4 apioNTPs while inducing partial primer degradation, and Phanta Max showed no detectable elongation. These results confirm that Therminator is uniquely efficient among the tested commercial enzymes for DNA-templated ApioNA synthesis.

We next examined the substrate preferences of Therminator by evaluating individual apioNTP incorporation on a 5N polynucleotide template (Figure **S2**). In the absence of Mn^{2+}, pyrimidine apioNTPs (T and C) stalled at the +2 position, while purine apioNTPs enabled complete extension with minor over-extension. Supplementing reactions with Mn^{2+} restored full-length product formation for all four apioNTPs. Mn^{2+} is known to relax polymerase substrate specificity via strengthened coordination with the β- and γ-phosphates of incoming nucleotides.[39] Consistently, purine apioNTPs exhibit markedly higher incorporation efficiency than pyrimidine analogs. This discrepancy likely arises from enhanced π-π stacking interactions, a structural feature previously characterized in pTNA and TNA systems.[19, 37]

2.2 Achieving Full-length ApioNA Synthesis and Reverse Transcription

To generate longer ApioNA oligonucleotides for subsequent fidelity studies, primer extension assays were initially performed using the 4NT9G template, a well-designed sequence previously used in the study of TNA replication.[37] Flanked by fixed primer-binding sites, this template features a central region minimizing continuous GG sequences to mitigate polymerase stalling while incorporating diverse nucleotide combinations around a central G residue. Unfortunately, primer extension assays utilizing the 4NT9G template failed to yield full-length ApioNA products across all tested conditions, including varied incubation durations, reaction temperatures, and polymerase concentrations.

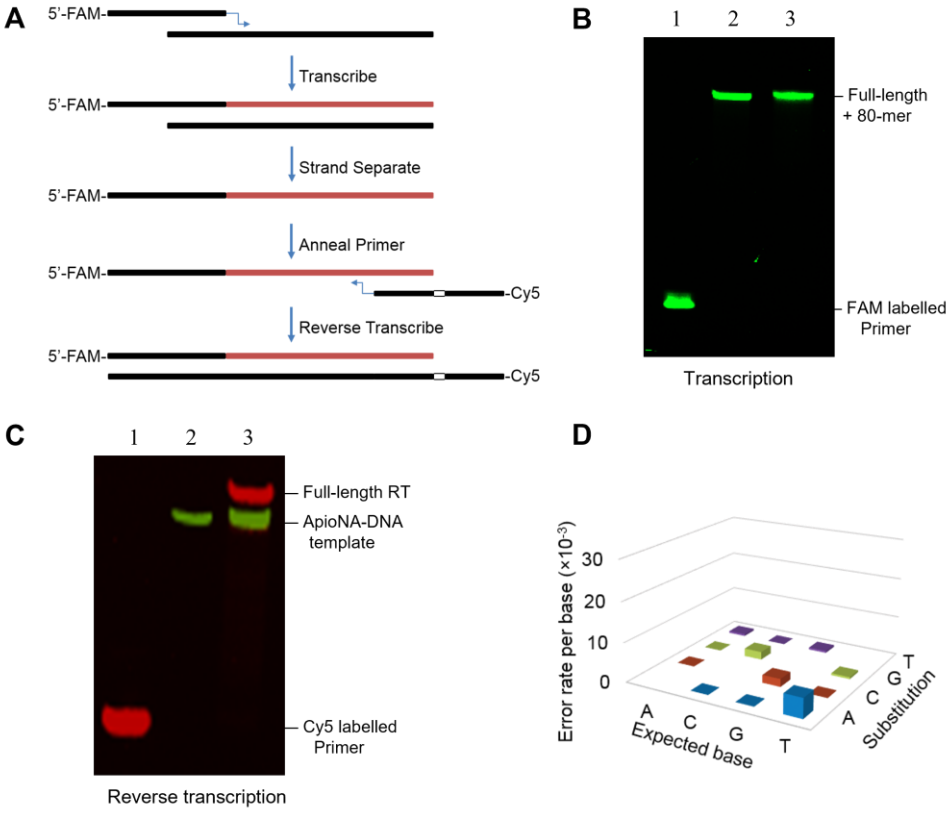

Figure 2. (**A**) Schematic representation of ApioNA synthesis and reverse transcription. ApioNA (red strand), DNA (black strand) and spacer 18 (blank strand). (**B**) Therminator-mediated ApioNA transcription reactions performed for 1 h at 37 °C and analyzed by denaturing polyacrylamide gel electrophoresis. Lane 1, FAM labelled primer; lane 2, dNTPs; lane 3, apioNTPs. (**C**) Bst 3.0-mediated ApioNA reverse transcription performed for 1 h at 50 °C and analyzed by denaturing polyacrylamide gel electrophoresis. Lane 1, Cy5 labelled primer; lane 2, purified ApioNA-DNA oligo from transcription; lane 3, reverse transcription with dNTPs. (**D**) Fidelity measurements of ApioNA replication cycle. The overall error rate is 20.5 x 10^{-3} (98.0% fidelity).

To overcome this limitation, we designed a biased pyrimidine-rich template (4NT5G, 80 nt, 77.5% T/C) to favor incorporation of the more efficiently polymerized purine

apioNTPs. With this optimized template, Therminator polymerase efficiently synthesized the complete 80-mer ApioNA strand without detectable truncated products (Figure **2B**). Reverse transcription from the synthetic ApioNA back into DNA was also successfully achieved by using a panel of commercial polymerases, including Bst 3.0, which gave the highest yield (Figure **S3**). Extending the reverse transcription primer from 20 to 40 nucleotides further improved efficiency, enabling the generation of full-length cDNA (Figure **2C**).

Finally, a complete DNA→ApioNA→DNA enzymatic replication cycle was established by using Therminator polymerase for forward polymerization and Bst 3.0 for reverse transcription. The fidelity of this cycle was quantified by PCR amplification of the cDNA, cloning into *E. coli*, and Sanger sequencing of over 1000 nucleotide positions from independent clones. The analysis revealed an aggregate error rate of approximately 20.5 × 10^{-3} per nucleotide incorporation, corresponding to a fidelity of 98.0% (Figure **2D** and Figure **S5**). This error rate is comparable to that of pTNA (17 × 10^{-3}), the closely related structural homolog that differs only in the exchange of CH_2 and O.[19]

2.3 *In vivo* processing of ApioNA by *E. coli*

Given that Bst 3.0 (a family A DNA polymerase) can reverse transcribe ApioNA *in vitro*, we examined whether *E. coli*'s native replication machinery could recognize ApioNA as a template for enzymatic polymerization within live bacterial cells. We constructed a pACYCDuet plasmid in which the His192 codon of the chloramphenicol resistance (CmR) gene was replaced by one, two, or three consecutive ApioNA residues (Figure **S6**). After transformation into *E. coli* DH5α, survival on chloramphenicol indicated transliteration of ApioNA into DNA by endogenous polymerases. Plasmids with one or three ApioNA substitutions yielded colony counts comparable to the wild-type control, and Sanger sequencing confirmed faithful restoration of the His192 sequence along with a silent watermark mutation (Figure **S7**). These results demonstrate that *E. coli* DNA polymerases can polymerize DNA using at least three consecutive ApioNA residues as a template, highlighting the polymer's compatibility with cellular machinery.

3. Hybridization Properties of ApioNA

To systematically evaluate the effect of ApioNA on the hybridization properties of duplexes, we synthesized a series of oligos including single ApioNA modified DNA duplexes, homopolymeric ApioNA AT sequences, and ApioNA strands incorporating all four ApioNA nucleosides. The thermal stability of homo-duplexes of these strands as well as hybrid-duplexes with DNA, RNA, and TNA was assessed by monitoring the melting temperature (T_m) using UV spectroscopy. Sequences of all oligos studied, T_m data, and the corresponding melting curves are provided in Table 1-2 and the Supplementary File.

3.1 Single ApioNA Residue Incorporation Destabilizes DNA Duplexes

To probe the impact of ApioNA on local structure, we first introduced single ApioNA residues (as A or T analogs) into the central position of either strand of a 13-mer DNA duplex. This incorporation proved disruptive to the duplexes, reducing the T_m values by 5.4 to 7.0 °C. This destabilization was dramatically stronger than that caused by TNA modifications (ΔT_m = -0.4 to -1.1 °C) in the same context. The stark contrast was further highlighted by incorporating a fully matched XNA–XNA pair to the central position of the DNA helix. While a TNA–TNA pair caused only a minor T_m reduction (ΔT_m = -2.6 °C),[40] an ApioNA–ApioNA pair of the same sequence led to a profoundly changed ΔT_m of -11.2 °C. This ~4-fold greater destabilization underscored a fundamental structural incompatibility between the ApioNA backbone and the canonical B-form DNA helix.

Table 1. T_m data of DNA duplexes containing single ApioNA or TNA.

T_m[a] and ΔT_m[b] (°C)	5'-d(ACT CAA ***T*** AGC CGT)-3'		
3'-d(TGA GTT ***A*** TCG GCA)-5'	DNA-**T**	ApioNA-**T**	TNA-**T**[c]
DNA-**A**	**60.5**	**53.5 / -7.0**	**60.1 / -0.4**
ApioNA-**A**	**55.1 / -5.4**	**49.3 / -11.2**	**—**
TNA-**A**[c]	**59.4 / -1.1**	**—**	**57.9 / -2.6**

[a]Measurements were performed at 260 nm with 2.5 μM of each complementary strand at a heating rate of 0.6 °C/min in1 M NaCl, 10 mM $MgCl_2$ and 10 mM Na-cacodylate (pH 7.0). The values of T_m (°C) represent an average of at least two separate experiments; [b]ΔT_m was calculated as $T_m^{\text{modified duplex}}$ - $T_m^{\text{unmodified duplex}}$. [c] Ref. 40; ***T*** indicates DNA-T, ApioNA-T, TNA-T, respectively; ***A*** indicates DNA-A, ApioNA-A, TNA-A, respectively; normal black letters indicate DNA. —: Not determined.

3.2 ApioNA Exhibits a Unique and Selective Hybridization Profile

Uncovering the disruptive nature of single ApioNA substitutions, we sought to further characterize the pairing capability of full ApioNA oligos. Initial experiments with homopolymeric ApioNA A and T showed no detectable duplex formation, which could be probably due to sequence-specific effects. We thereafter conducted a more rigorous analysis using fully modified, mixed-sequence oligonucleotides incorporating all four ApioNA nucleobases.

Table 2. T_m[a] data of DNA, RNA, TNA and ApioNA: homoduplexes and heteroduplexes.

3'-(AAT ATA AAT TTT)-5'	5'-(TTA TAT TTA AAA)-3'			
	DNA	RNA[b]	ApioNA	
DNA	**31.5**	**16.7**	***I***	
RNA[b]	**19.2**	**31.3**	***I***	
ApioNA	***I***	***I***	***I***	
3'-GTC CAG TGA TGC-5'	**5'-CAG GTC ACT ACG-3'**			
	DNA	RNA[b]	TNA	ApioNA
DNA	**57.8**	**56.3**	**53.5**	**17.9**[c]
RNA[b]	**54.5**	**68.1**	**62.9**	**39.5**
TNA	**52.9**	**62.5**	**63.1**	**29.0**
ApioNA	**12.2**[c]	**41.9**	**26.2**	**7.5**[c]

[a] Measurements were performed at 260 nm with 2.5 µM of each complementary strand at a heating rate of 0.6 °C/min in1 M NaCl, 10 mM $MgCl_2$ and 10 mM Na-cacodylate (pH 7.0). The values of T_m represent an average of at least two separate experiments. [b]Oligonucleotide U base instead of T base. [c]The heating curves exhibit only a segment of the sigmoidal curve. ***I***: complex not stable enough to be detected. The labels 5' and 3' denote strand orientation in DNA and RNA sequences, for TNA and ApioNA sequences, the corresponding labels are 3' and 2'.

ApioNA Homoduplexes Are Exceptionally Weak. The fully modified ApioNA strand formed an extremely unstable homoduplex, exhibiting a T_m of only 7.5 °C. In stark contrast, a TNA homoduplex of the same sequence has a T_m of 63.1 °C, while DNA and RNA homoduplexes have T_m values of 57.8 °C and 68.1 °C, respectively. These findings underscore that ApioNA is deficient in self-complementarity required for stable duplex formation under normal conditions (e.g. at room temperature).

ApioNA-DNA Heteroduplexes Are Highly Thermally Unstable. ApioNA also showed minimal affinity for DNA. The T_m values of ApioNA:DNA heteroduplexes were 12.2 °C

(ApioNA strand with complementary DNA) and 17.9 °C (DNA strand with complementary ApioNA), indicating significant destabilizations relative to the DNA-DNA homoduplex (T_m = 57.8 °C). These low T_m values confirm that ApioNA is essentially orthogonal to DNA under physiological conditions.

ApioNA-RNA Heteroduplexes Show Moderate Thermal Stability. In stark contrast to the very unstable ApioNA-DNA duplexes, ApioNA formed a moderately stable duplex with complementary RNA ($T_m \approx 40$ °C), revealing a significant base-pairing selectivity for RNA over DNA. This suggests that the ApioNA backbone may be better accommodated by the A-form geometry of RNA than that of B-form DNA.

ApioNA-TNA Heteroduplexes Exhibit Detectable Hybridization. Interestingly, ApioNA also formed heteroduplexes with TNA, with T_m values of 26.2 °C and 29.0 °C, respectively. Although they were approximately 10 °C less stable than ApioNA-RNA heteroduplexes, these values were close to room temperature, significantly higher than those of ApioNA-DNA heteroduplexes, which again suggests that ApioNA backbone is selective for A-form geometry for hybridization since TNA is considered as an RNA analogue preferentially adopting A-form geometry.[3]

3.3 Circular Dichroism Reveals Structural Adaptability of ApioNA Duplexes

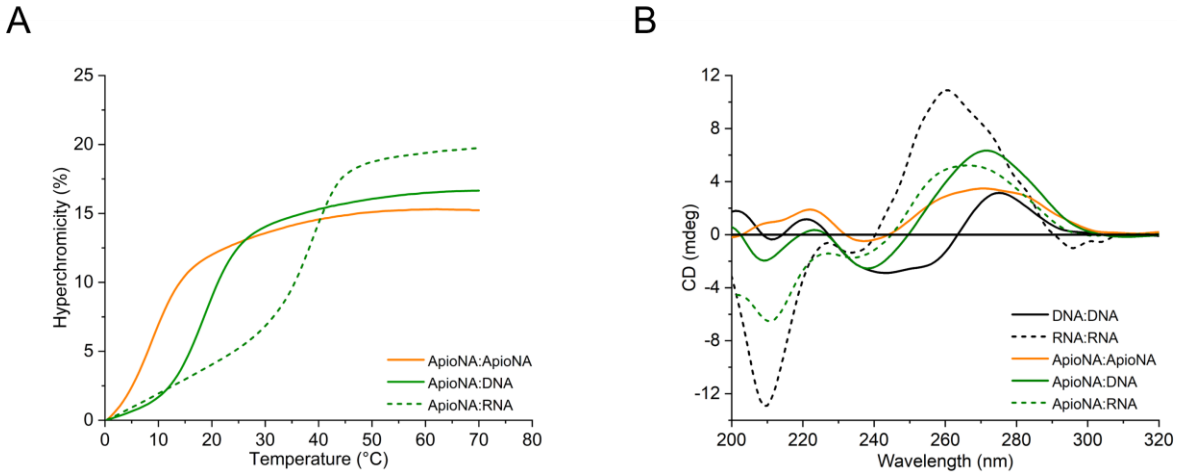

Figure 3. (**A**) Melting curves of fully modified ApioNA and hybrid ApioNA:DNA and ApioNA:RNA duplexes. (**B**) CD spectra of fully modified and hybrid ApioNA duplexes, along with their hybrids formed with complementary DNA or RNA strands, in comparison to natural dsDNA and dsRNA; spectra were measured at 5 °C (ApioNA:ApioNA and ApioNA:DNA) or 25 °C (DNA:DNA, RNA:RNA and ApioNA:RNA), and are shown in units of molar ellipticity as a function of wavelength; the ApioNA strand refers to the **ON5**, the complementary ApioNA strand (**ON6**) and its CD spectra are provided in Table **S1** and Figure **S8**, respectively.

To understand the pairing selectivity of ApioNA for RNA over DNA, we characterized the secondary structures of ApioNA-containing duplexes with DNA, RNA, and with itself by using circular dichroism (CD) spectroscopy (Figure **3** and Figure **S8**). Due to the low thermal stability of double-stranded ApioNA (ds) and ApioNA:DNA hybrids (both with T_m < 20 °C, Figure **3A**), we measured their CD spectra at 5 °C to preserve their folded conformations. Other duplexes were recorded at 25 °C (Figure **3B**). The DNA and RNA duplex controls exhibited canonical CD profiles: dsDNA (B-form) displayed a positive peak between 260 and 280 nm and a negative band near 245 nm, while dsRNA (A-form) showed a strong positive peak at 260 nm and a prominent negative band around 210 nm.[41]

The ApioNA homoduplex exhibited a broad positive signal spanning 240–300 nm, with a maximum at 270 nm. While its overall spectral shape resembled B-form DNA, differences in peak position and intensity may indicate a unique helical architecture. In contrast, the ApioNA–DNA hybrid displayed a CD profile closely mirroring that of B-form DNA, featuring a positive peak at 272 nm and a negative band at 238 nm. The ApioNA–RNA hybrid, however, showed a spectral pattern nearly identical to A-form RNA, with a positive peak at 266 nm and a negative band at 210 nm, though with reduced intensity. These results suggest that the global helical geometry of ApioNA-containing duplexes is primarily influenced by the complementary strand—DNA or RNA—rather than by ApioNA itself. This structural adaptability implies conformational flexibility of the ApioNA backbone (particularly the sugar pucker), allowing it to accommodate the helical preferences of its pairing partner.

4. Enhanced Nuclease Resistance of ApioNA

To assess nuclease stability, ApioNA and control DNA oligonucleotides were incubated with snake venom phosphodiesterase (SVPD) or 50% human serum (HS) at 37 °C. Reaction aliquots were collected at predetermined time points, quenched and analyzed via denaturing polyacrylamide gel electrophoresis (PAGE). Control DNA underwent rapid degradation, with half-lives of approximately 5 min in SVPD and 8 min in HS (Figure **S9**). In marked contrast, ApioNA displayed greatly extended half-lives of 3.9 h and 39.8 h in SVPD and HS, respectively—roughly 50-fold and 300-fold longer than DNA. These results confirm that ApioNA possesses outstanding nuclease resistance and is capable of prolonged stability in biological environments.

5. Computational Insights into ApioNA Structure and Interactions

5.1 Structural and energetic basis for the hybridization of ApioNA with DNA or RNA

Our thermodynamic and CD studies revealed distinct hybridization properties of ApioNA with DNA and RNA and the CD spectra indicated potential relation to the conformational flexibility of the ApioNA backbone, particularly the sugar pucker. To characterize ApioNA puckering conformations, we employed an established quantum mechanical (QM) approach[42] to construct 2D potential energy surfaces (PESs) via systematic scanning of Cartesian coordinates Z_x and Z_y (Figure **4A** and **4B**). Furanose ring PESs are typically non-rugged, with stable conformations residing in broad basins around Z_x = ±30° and Z_y = ±30°;[43] we therefore initiated geometry optimizations from 8 initial structures at the intersections of these lines and the coordinate axes (Z_x=0°, Z_y=0°). The HF-3c method—known to reliably reproduce PESs from more computationally expensive QM calculations—was used for these optimizations.[44]

Our optimizations of apio-nucleoside monophosphates demonstrated that all four apio-nucleotides converge to two primary puckering states (Figure **4C**). The most stable conformation exhibited a phase angle near 33°, classified as the $^{3}\boldsymbol{T}_{4}$ (C3'-endo/C4'-exo) twist conformation, close to the North-type pucker typical of RNA. A secondary, less stable conformation adopted the $^{4}\boldsymbol{T}_{3}$ (C4'-endo/C3'-exo) twist pucker (South-type), with a small energy difference of ~ 1.1 kcal/mol that permits substantial ring flexibility at room temperature. By comparison, experimental studies on TNA, including crystal structures and solution NMR data, consistently identify an average C4'-exo geometry as the preferred threose sugar conformation.[45] In contrast, the phosphonate-linked pTNA, a structural isomer of ApioNA, exhibits a rigid single-pucker state, locked exclusively in the $^{1}\boldsymbol{T}_{o}$ (C1'-endo/*O*4'-exo) conformation in molecular dynamics simulations.[44]

To further understand how ApioNA forms duplexes with itself, DNA or RNA, we performed systematic *ab initio* calculations on trinucleotide duplexes representing GC-rich (GCG:CGC, CCG:CGG) and AT-rich (ATA:TAT, TTA:TAA) sequences, initially constructing the ApioNA strands in the $^{3}\boldsymbol{T}_{4}$ twist conformation. In all ApioNA homoduplexes, ApioNA residues consittently showed puckering alternation between $^{o}\boldsymbol{T}_{4}$ and $^{4}\boldsymbol{T}_{o}$ (or closely related puckers) states, reflecting the high conformational flexibility of ApioNA homoduplexes. This dynamic interconversion between two puckering states, rather than a single stable conformation, may account for the absence of detectable ApioNA homoduplexes. In ApioNA:RNA hybrids, the RNA sugar uniformly adopted the canonical

C3′-endo (A-form) pucker, while the ApioNA sugar remained in the stable $^{o}\boldsymbol{T}_{4}$ conformation; both strands adopted their respective energy-minimum puckering states, yielding stable duplexes with minimal energetic penalty. Notably, attempts to model ApioNA:DNA duplexes with the $^{3}\boldsymbol{T}_{4}$ twist conformation revealed significant mismatching between strands, with the C1′···C1′ distances in the ApioNA strand being substantially larger than those in DNA, indicating poor geometric compatibility (Figure **S10**). When we instead employed the less stable $^{4}\boldsymbol{T}_{3}$ pucker for the ApioNA strand, the optimized ApioNA:DNA duplexes (Figure **4E** and **4F**) showed the ApioNA nucleotides adopting the $^{4}\boldsymbol{T}_{o}$ conformation, while the DNA strand adopted C2′-endo or closely related geometry, thus forming a typical B-form helix—features consistent with our CD spectra. Compared with ApioNA:RNA hybrids, where both strands adopt favorable conformations, the ApioNA:DNA hybrids force the ApioNA sugar into a higher-energy secondary puckering ($^{4}\boldsymbol{T}_{o}$), raising the energetic cost and resulting in lower stability, in full agreement with our experimental T_m measurements.

In addition, we measured the intrastrand P···P distance of ApioNA in the QM-optimized trinucleotide duplexes, which spans 6.0-7.0 Å, reflecting the enhanced backbone flexibility conferred by the extra methylene group. For comparison, TNA exhibits a fixed P–P spacing of approximately 5.7-5.9 Å in its duplex structures,[45] whereas DNA and RNA typically show distances of ~6.8 and ~6.0 Å, respectively.[46-47]

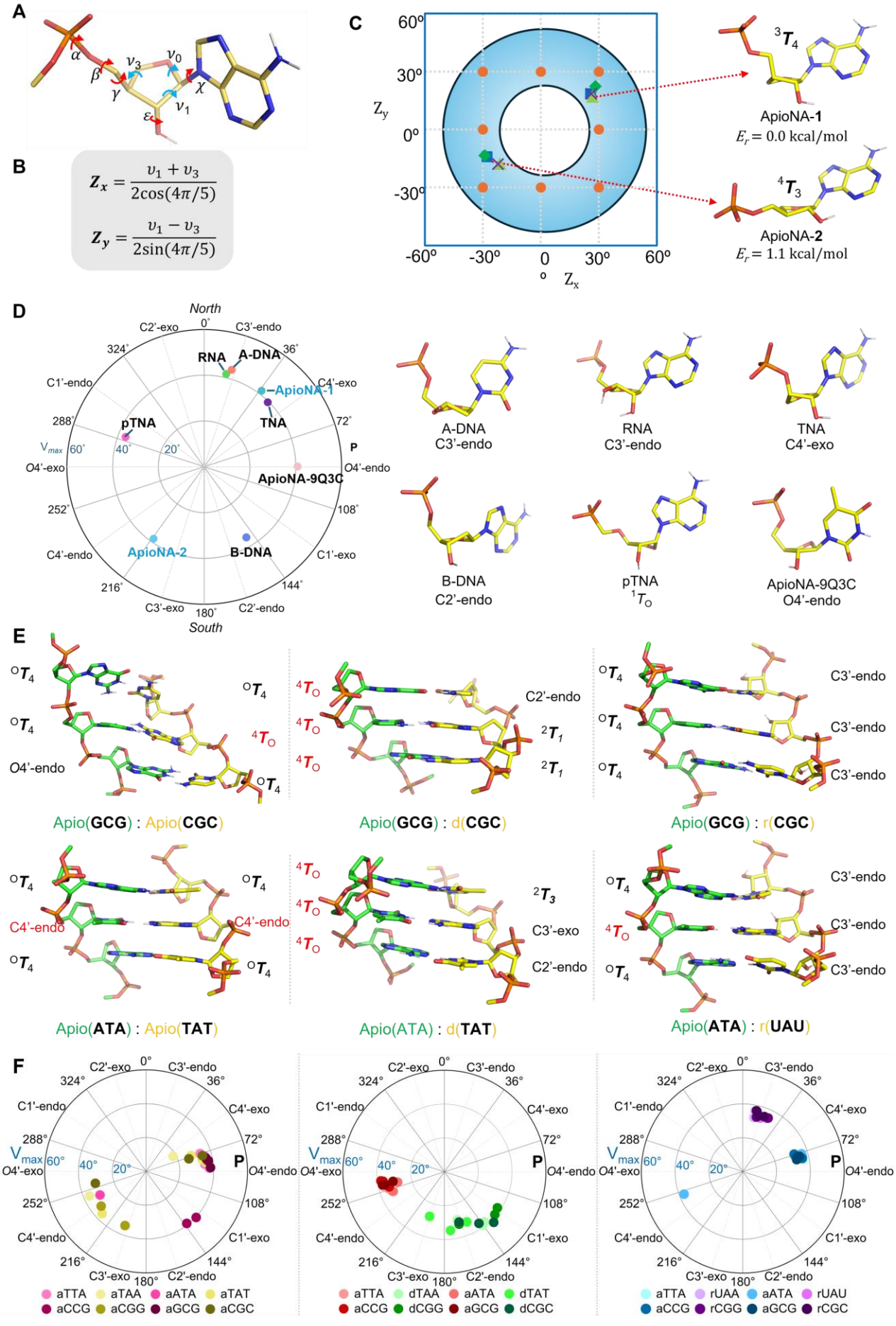

Figure 4. **Computational sampling the puckering conformations of apioNA sugar ring.** (**A**) The molecule model used for pucker sampling. Only apioA monophospate is shown here. The intra-ring dihedrals of the sugar are indicated by cyan curved arrows. The backbone and glycosidic dihedrals (α, β, γ, ε and χ) are indicated by red arrows. (**B**) The definitions of the Cartesian coordinates Z_x and Z_y. (**C**) Distribution of initial and optimized geometries of apioNA nucleotides on the Z_x-Z_y PES contour. The light-blue doughnut-shaped ring indicates the region where energy minima are probably located. Orange dots indicate the initial geometries of apio-nucleotides, while blue square, green diamond, light-green triangle, and purple cross indicate optimized geometries of apio-A, apio-G, apio-C and apio-T, respectively. The optimized geometries of apio-A are presented with the classification of puckering conformations indicated. E_r: Relative Energy (with respect to the global minimum). (**D**) Puckering conformations of nucleic acid sugar rings. Optimized geometries of apioNA nucleotides on the pseudorotation wheel of suger puckering. Sugar puckering conformations of well studies natural and artificial nucleic acids. (**E**) QM calculated structural models of duplexes of ApioNA, DNA and RNA trinucleotides. GC-rich duplexes (GCG:CGC) of ApioNA/ApioNA, ApioNA/DNA and ApioNA/RNA; AT-rich duplexes (ATA:TAT; for RNA: UAU) of ApioNA/ApioNA, ApioNA/DNA and ApioNA/RNA. (**F**) Sugar puckering conformations of ApioNA, DNA, and RNA trinucleotide duplex models on the pseudorotation wheel.

5.2 Recognition of apioNTPs by Therminator DNA polymerase

Since ApioNA differs from DNA in both chemical structures and puckering conformations, a question arose that how the Therminator DNA polymerase recognized apioNTPs, although this enzyme has been reported to be capable to incorporate a variety of modified nucleotides.[38] To answer this question, we carried out computational modeling studies on the interactions between apioNTPs and Therminator (Figure **5A**).

Molecular modeling results revealed that apioNTPs adopted a binding pose analogous to the natural substrate dATP (Figure **5B**): the base formed correct pairs with the DNA template, and the triphosphate moiety coordinated with the catalytic metal center (Mg^{2+}-Mn^{2+}-Mg^{2+}) (Figure **S13**). The α-phosphate of all apioNTPs aligned nearly identically to that of dATP, with a 3.5–3.9 Å distance between the primer's 3'-O and the apioNTP's α-phosphorus; the O3' atom was also positioned opposite the oxygen bridging the α- and β-phosphates—a trans-alignment prerequisite for catalysis.[48]

Further analysis focused on polymerase recognition of the ApioNA scaffold (Figure **5C**). In the dATP-bound structure, the deoxyribose (C3'-endo) packs against Y409, with C2' positioned closest to the phenol ring (a 2'-OH group at this position would induce steric clash).[49] However, the O4'-endo pucker of ApioNA displaces the C2' atom away from Y409, creating space for the 2'-OH. Additionally, the ApioNA sugar ring rotates ~40° toward the

metal center, enabling the 2'-OH to form stabilizing H-bonds with the Y409 backbone and N491 side chain. These findings explain the enzyme's ability to accommodate and utilize apioNTPs.

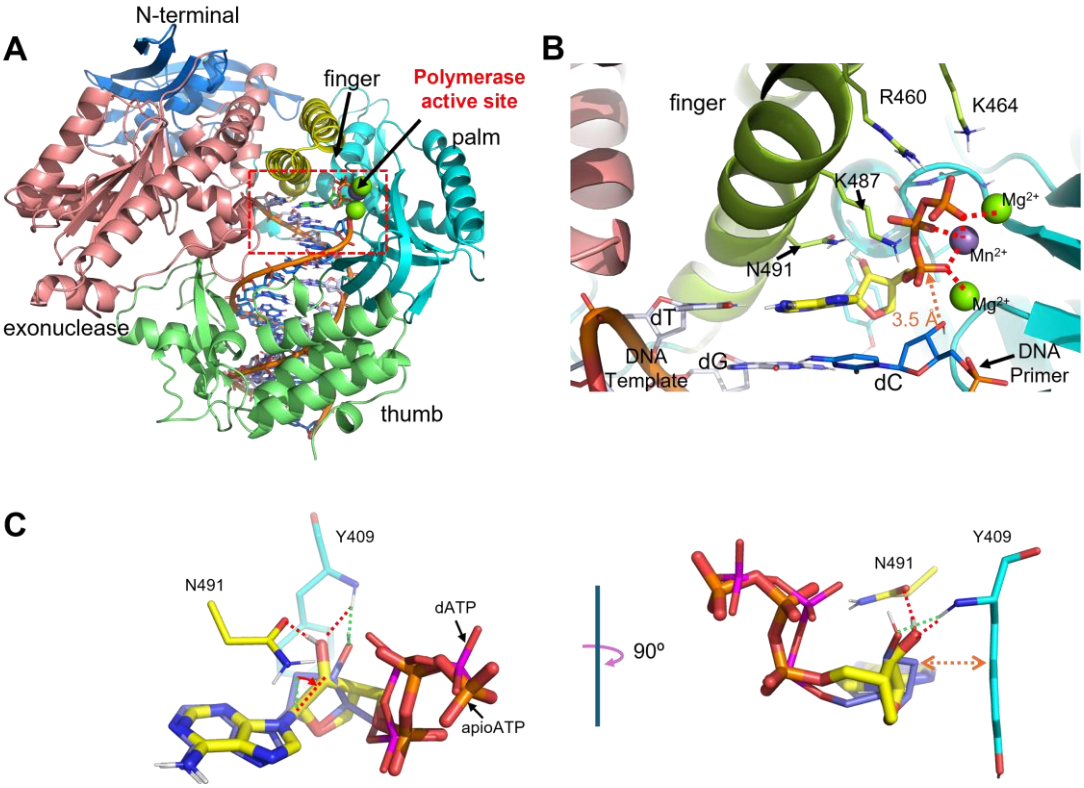

Figure 5. Ternary models of DNA polymerase, DNA Primer:Template (PT) duplex and incoming apioNTPs at the catalytic site of the DNA polymerase. (**A**) Overall structure of 9°N DNA polymerase, DNA PT duplex and apioATP. The polymerase was colored in blue, pink, limon, cyan and green for the *N*-terminal, exonuclease, finger, palm and thumb domains, respectively. (**B**) The detailed binding interactions of incoming apioATP with the catalytic sites of the polymerase-DNA PT duplex ternary complex. The dashed yellow arrows indicated the distances between O3' atom of the DNA primer and the α-phosphorus of apioNTPs. (**C**) Overlay of apioATP (thicker sticks) and dATP (thinner sticks) at the catalytic site. The interactions between NTPs and the "steric gate" residue Y409 (cyan) were depicted. ApioNTPs were shown with carbon atoms colored in yellow. Key amino acid residues of the polymerase and DNA nucleotides were also shown as sticks. Particularly, carbons atoms of the template DNA were colored in lightgray, while carbons of the primer were colored in lightblue. Other atoms including N, O, H and P were colored in blue, red, light-gray and orange, respectively. Mg^{2+} and Mn^{2+} ions were shown as green and gray spheres, respectively.

Discussion

Our comprehensive investigation of ApioNA establishes it as a distinct member of the XNA family with intrinsically biased RNA-selective hybridization properties. In contrast to fully compatible XNAs such as TNA that readily form stable duplexes with both DNA and RNA, and orthogonal XNAs exemplified by pTNA that largely abolish cross-hybridization with natural nucleic acids, ApioNA exhibits unambiguous pairing preference toward RNA. Fully modified ApioNA oligomers assemble moderately stable duplexes with complementary RNA sequences, while forming only weak DNA heteroduplexes and negligible homoduplex structures.

The unique pairing selectivity of ApioNA originates from the characteristic conformational behavior of its apiofuranose scaffold, which integrates partial structural features of both TNA and pTNA. Previous structural studies of TNA, including crystallographic and solution NMR characterizations of TNA-containing duplexes, have validated a “close to C4’-exo” conformation (or its twisted $^{3}\boldsymbol{T}_{4}$ form), as its thermodynamically favored conformation.[45] By comparison, molecular dynamics simulations of pTNA reveal that its threose ring is conformationally restricted to a fixed $^{1}\boldsymbol{T}_{O}$ pucker across all duplex states. The phosphonomethyl-modified backbone imposes severe geometric constraints, locking pTNA into a single high-energy sugar conformation.[44]

In contrast, our QM calculations of ApioNA monophosphates identify two thermodynamically favorable puckering states. The predominant $^{3}\boldsymbol{T}_{4}$ conformation closely matches the canonical sugar geometry of A-form helices, whereas the minor population adopts the $^{4}\boldsymbol{T}_{3}$ twist pucker (South-type). Despite occupying opposite regions on the pseudorotation wheel, these two conformations differ by merely ~1.1 kcal/mol, indicating the apiofuranose ring prominent structural flexibility. This conformational versatility is further underscored by a high-resolution crystal structure of an RNA duplex containing a single ApioNA residue, in which the apiofuranose sugar adopts an O4’-endo (East-type) pucker. While in the same study, computational modeling of ApioNA embedded within B-form DNA confirms the adoption of a C4’-exo puckering mode.[25]

Structural modeling of ApioNA-containing trinucleotide duplexes further demonstrates that the nucleoside-preferred $^{3}\boldsymbol{T}_{4}$ conformation can undergo subtle geometric rearrangement toward the $^{O}\boldsymbol{T}_{4}$ pucker within duplex environments (Figure **S14**, distribution of puckers in QM-optimized trinucleotide duplexes). Such conformational adaptation enables stable pairing between ApioNA and RNA strands. Conversely, combination of

ApioNA in the $^{3}\boldsymbol{T}_{4}$ pucker with canonical B-form DNA induces severe base-pair mismatching and non-planar duplex geometry. Although ApioNA can adopt a secondary minimum energy state $^{4}\boldsymbol{T}_{3}$ to accommodate DNA pairing via rearrangement to the $^{4}\boldsymbol{T}_{\mathrm{O}}$ pucker, this process requires a notable increase in conformational energy. The inherent energetic penalty partially accounts for the weakened DNA-binding capacity of ApioNA relative to RNA. For ApioNA homoduplexes, ApioNA residues display alternating $^{\mathrm{O}}\boldsymbol{T}_{4}/^{4}\boldsymbol{T}_{\mathrm{O}}$ puckering, reflecting high flexibility and the absence of a dominant low-energy conformation, which results in very weak self-pairing. Thus, these findings suggest that ApioNA can sample multiple low-energy puckering modes governed by sequence context and pairing partner, with a low conformational interconversion barrier.

In addition to the conformational adaptability of the sugar ring, the extra methylene group between C3' and O3' provides the ApioNA backbone with greater conformational freedom.[50] Our computational modeling illustrates this enhanced backbone flexibility: the intrastrand P···P distance of ApioNA spans 6 to 7 Å, allowing the phosphate chain to contract or elongate and fit diverse helical conformations. In comparison, TNA possesses a shorter backbone repeat with P···P distances of roughly 5.7–5.9 Å.[45] This fixed spacing restricts backbone mobility and locks duplex assemblies into an A-type geometry for paired strands. The dual flexibility of ApioNA—adjustable sugar puckering alongside variable phosphate separation—aligns closely with our CD spectroscopic measurements. ApioNA-RNA hybrid duplexes produce characteristic A-form spectral signals, whereas ApioNA-DNA heteroduplexes adopt B-form conformations shaped primarily by the DNA strand. Notably, 2',5'-linked nucleic acids also display intrinsic RNA pairing preference.[51-52] This selectivity arises from backbone O2' atoms that stabilize A-form-like helical arrangements.[53] The same structural rule likely applies to ApioNA, as its phosphate backbone retains conserved O2' functional groups.

Surprisingly, ApioNA's weak solution-phase compatibility with DNA does not hinder its enzymatic assembly and replication, representing a mechanistic analogy to previously reported pTNA systems.[54] Prior studies have confirmed that polymerases can serve as molecular clamps to override weak intrinsic duplex stability, forcing constrained XNA residues into canonical Watson–Crick base pairing. Our molecular docking analyses support a similar clamping mechanism for ApioNA. ApioNTPs closely mimic the binding pose of native dATP, wherein the O4'-endo sugar pucker optimizes active-site positioning and facilitates hydrogen bond formation with the catalytic metal center. The synergy between active-site confinement and specific molecular interactions enables efficient enzymatic synthesis of weakly DNA-compatible ApioNA strands. Unlike pTNA, which

strictly depends on engineered polymerase mutants for strand assembly, ApioNA can be efficiently elongated by commercial Therminator polymerase to produce full-length oligonucleotides. This enzymatic strategy circumvents the inherent length constraints of conventional solid-phase chemical synthesis and creates ample opportunities for future functional investigations.

The conformational adaptability of ApioNA also confers broad enzymatic compatibility and replicability. Both Family B Therminator and Family A Bst 3.0 polymerases support complete DNA→ApioNA and ApioNA→DNA chain transfer, reconstituting a full in vitro replication cycle with a high fidelity of 98.0%. The measured error rate is comparable to that of well-characterized pTNA systems. Beyond dedicated replication polymerases, engineered TNA polymerases also tolerate apioNTP incorporation to generate chimeric ApioNA/TNA strands, further verifying the adaptive substrate compatibility of the apiose scaffold.[25] Consistent with this flexible substrate tolerance, our results also enable the efficient synthesis of ApioNA/DNA chimeric oligonucleotides via single-nucleotide substitution of dNTPs with apioNTPs. Most importantly, native *E*. coli replication machinery is capable of faithfully transliterating consecutive ApioNA residues into DNA, restoring cellular antibiotic resistance. This unique property establishes ApioNA as a rare non-orthogonal XNA compatible with endogenous biological systems.

In summary, ApioNA's unique RNA-selective hybridization profile is governed by its intrinsic sugar conformational flexibility and the enhanced backbone flexibility conferred by the extra methylene group in the internucleotide linkage. The adjustable sugar puckering and variable phosphate separation together define a dual flexibility that is fully consistent with our CD spectroscopic measurements, where ApioNA–RNA hybrids adopt A-form geometry while ApioNA–DNA heteroduplexes assume B-form features dictated by the DNA strand. Despite weak solution-phase DNA affinity, ApioNA is amenable to efficient enzymatic replication by both engineered and native polymerases. These distinct structural and functional properties render ApioNA a promising platform for RNA-targeted applications and therapeutics, where minimal DNA cross-reactivity is essential. ApioNA represents a prototype for selective RNA recognition, expanding the chemical diversity of the XNA functional spectrum. Our work validates sugar conformation and backbone flexibility as joint design parameters for programming nucleic acid interaction specificity. More broadly, this study may provide future inspiration and insight for creating XNAs with tailored recognition properties, opening new avenues for synthetic biology and molecular medicine where precise discrimination between nucleic acid targets is required.

Acknowledgements

We thank members of the Mei laboratory for helpful suggestions and comments on the manuscript. This work was supported by the following funding: Shenzhen Medical Research Fund (E250200213), National Key R&D Program of China (Grant No. 2022YFF1201800), Guangdong Basic and Applied Basic Research Foundation (2026A1515012013), Guangdong Provincial Key Laboratory of Synthetic Genomics (2023B1212060054); Shenzhen Key Laboratory of Synthetic Genomics (SYSPG20241211173920047); Shenzhen Institute of Synthetic Biology Scientific Research Program (JCHZ20210002). We are grateful to the Shenzhen Infrastructure for Synthetic Biology and National Industrial Innovation Center for Bio-manufacturing for instrument support and technical assistance.

Supplemental Information. This file contains

Competing Interests Statement. The authors declare no competing financial interests.

References:

1. Handal-Marquez, P.; Anupama, A.; Pezo, V.; Marlière, P.; Herdewijn, P.; Pinheiro, V. B., Beneath the XNA world: Tools and targets to build novel biology. *Current Opinion in Systems Biology* **2020,** *24*, 142-152.

2. Freund, N.; Fürst, M. J. L. J.; Holliger, P., New chemistries and enzymes for synthetic genetics. *Current Opinion in Biotechnology* **2022,** *74*, 129-136.

3. Anosova, I.; Kowal, E. A.; Dunn, M. R.; Chaput, J. C.; Van Horn, W. D.; Egli, M., The structural diversity of artificial genetic polymers. *Nucleic Acids Research* **2016,** *44* (3), 1007-1021.

4. Eschenmoser, A., Etiology of Potentially Primordial Biomolecular Structures: From Vitamin B12 to the Nucleic Acids and an Inquiry into the Chemistry of Life's Origin: A Retrospective. *Angewandte Chemie International Edition* **2011,** *50* (52), 12412-12472.

5. Chaput, J. C., Redesigning the Genetic Polymers of Life. *Accounts of Chemical Research* **2021,** *54* (4), 1056-1065.

6. Chaput, J. C.; Egli, M.; Herdewijn, P., The XNA alphabet. *Nucleic Acids Res* **2025,** *53* (13).

7. Taylor, A. I.; Pinheiro, V. B.; Smola, M. J.; Morgunov, A. S.; Peak-Chew, S.; Cozens, C.; Weeks, K. M.; Herdewijn, P.; Holliger, P., Catalysts from synthetic genetic polymers. *Nature* **2014,** *518* (7539), 427-430.

8. Deleavey, Glen F.; Damha, Masad J., Designing Chemically Modified Oligonucleotides for Targeted Gene Silencing. *Chemistry & Biology* **2012,** *19* (8), 937-954.

9. Egli, M.; Manoharan, M., Chemistry, structure and function of approved oligonucleotide therapeutics. *Nucleic Acids Res* **2023,** *51* (6), 2529-2573.

10. Koshkin, A. A.; Nielsen, P.; Meldgaard, M.; Rajwanshi, V. K.; Singh, S. K.; Wengel, J., LNA (locked nucleic acid): an RNA mimic forming exceedingly stable LNA:LNA duplexes. *Journal of the American Chemical Society* **1998,** *120*, 13252-13253.

11. Berger, I.; Tereshko, V.; Ikeda, H.; Marquez, V. E.; Egli, M., Crystal structures of B-DNA with incorporated 2'-deoxy-2'-fluoro-arabino-furanosyl thymines: implications of conformational preorganization for duplex stability. *Nucleic Acids Res* **1998,** *26*, 2473-2480.

12. Manoharan, M.; Akinc, A.; Pandey, R. K.; Qin, J.; Hadwiger, P.; John, M.; Mills, K.; Charisse, K.; Maier, M. A.; Nechev, L.; Greene, E. M.; Pallan, P. S.; Rozners, E.; Rajeev, K. G.; Egli, M., Unique gene-silencing and structural properties of 2'-fluoro-modified siRNAs. *Angew Chem Int Ed Engl* **2011,** *50* (10), 2284-8.

13. Wang, Q.; Chen, X.; Li, X.; Song, D.; Yang, J.; Yu, H.; Li, Z., 2'-Fluoroarabinonucleic Acid Nanostructures as Stable Carriers for Cellular Delivery in the Strongly Acidic Environment. *ACS Appl Mater Interfaces* **2020,** *12* (48), 53592-53597.

14. Schoning, K.-U.; Scholz, P.; Guntha, S.; Wu, X.; Krishnamurthy, R.; Eschenmoser, A., Chemical etiology of nucleic acid structure: the alpha-threofuranosyl-(3' → 2') oligonucleotide system. *Science* **2000,** *290*, 1347-1351.

15. Pallan, P. S.; Wilds, C. J.; Wawrzak, Z.; Krishnamurthy, R.; Eschenmoser, A.; Egli, M., Why Does TNA Cross-Pair More Strongly with RNA Than with DNA? An Answer From X-ray Analysis. *Angewandte Chemie International Edition* **2003,** *42* (47), 5893-5895.

16. Yu, H.; Zhang, S.; Chaput, J. C., Darwinian evolution of an alternative genetic system provides support for TNA as an RNA progenitor. *Nature Chemistry* **2012,** *4* (3), 183-187.

17. Herdewijn, P., Nucleic acids with a six-membered 'carbohydrate' mimic in the backbone. *Chem Biodivers* **2010,** *7*, 1-59.

18. Wang, J.; Verbeure, B.; Luyten, I.; Lescrinier, E.; Froeyen, M.; Hendrix, C.; Rosemeyer, H.; Seela, F.; Aerschot, A. V.; Herdewijn, P., Cyclohexene Nucleic Acids (CeNA): Serum Stable Oligonucleotides that Activate RNase H and Increase Duplex Stability with Complementary RNA. *Journal of the American Chemical Society* **2000,** *122*, 8595-8602.

19. Liu, C.; Cozens, C.; Jaziri, F.; Rozenski, J.; Maréchal, A.; Dumbre, S.; Pezo, V.; Marlière, P.; Pinheiro, V. B.; Groaz, E.; Herdewijn, P., Phosphonomethyl Oligonucleotides as Backbone-Modified Artificial Genetic Polymers. *Journal of the American Chemical Society* **2018,** *140* (21), 6690-6699.

20. Maiti, M.; Maiti, M.; Knies, C.; Dumbre, S.; Lescrinier, E.; Rosemeyer, H.; Ceulemans, A.; Herdewijn, P., Xylonucleic acid: synthesis, structure, and orthogonal pairing properties. *Nucleic Acids Res* **2015,** *43* (15), 7189-200.

21. Luo, M.; Groaz, E.; Froeyen, M.; Pezo, V.; Jaziri, F.; Leonczak, P.; Schepers, G.; Rozenski, J.; Marlière, P.; Herdewijn, P., Invading Escherichia coli Genetics with a Xenobiotic Nucleic Acid Carrying an Acyclic Phosphonate Backbone (ZNA). *Journal of the American Chemical Society* **2019,** *141* (27), 10844-10851.

22. Kataoka, M.; Kouda, Y.; Sato, K.; Minakawa, N.; Matsuda, A., Highly efficient enzymatic synthesis of 3′-deoxyapionucleic acid (apioNA) having the four natural nucleobases. *Chemical Communications* **2011,** *47* (30), 8700.

23. Kataoka, M.; Sato, K.; Matsuda, A., Synthesis of 3'-deoxyapionucleoside triphosphates and their incorporation into DNA by DNA polymerase. *Nucleic Acids Symposium Series* **2008,** *52* (1), 281-282.

24. Toti, K. S.; Derudas, M.; Pertusati, F.; Sinnaeve, D.; Van den Broeck, F.; Margamuljana, L.; Martins, J. C.; Herdewijn, P.; Balzarini, J.; McGuigan, C.; Van Calenbergh, S., Synthesis of an Apionucleoside

Family and Discovery of a Prodrug with Anti-HIV Activity. *The Journal of Organic Chemistry* **2014,** *79* (11), 5097-5112.

25. Jauregui-Matos, V.; Datta, D.; Kundu, J.; Kumar, V.; Harp, J. M.; Adebayo, A.; Donnelly, D.; Medina, E.; Chaput, J. C.; Egli, M.; Manoharan, M., Synthesis and Biophysical Properties of 3'-Deoxy-beta-d-apio-d-furanosyl Nucleic Acids. *ACS Chem Biol* **2025,** *20* (11), 2698-2708.

26. Gao, Y.; Xiong, C.; Zhang, C.; Wen, J.; Chen, X.; Li, X.; Dai, Z.; Zhou, L.; Mei, H., 3'-C-Extended TNA: De Novo Synthesis, Enhanced Exonuclease Resistance, and Functional siRNA 3'-Overhang Modifications Without Compromising Gene Silencing. *Chemistry* **2025,** *31* (54), e02182.

27. Beddoe, R. H.; Andrews, K. G.; Magné, V.; Cuthbertson, J. D.; Saska, J.; Shannon-Little, A. L.; Shanahan, S. E.; Sneddon, H. F.; Denton, R. M., Redox-neutral organocatalytic Mitsunobu reactions. *Science* **2019,** *365* (6456), 910-914.

28. Swamy, K. C. K.; Kumar, N. N. B.; Balaraman, E.; Kumar, K. V. P. P., Mitsunobu and Related Reactions: Advances and Applications. *Chemical Reviews* **2009,** *109*, 2551-2651.

29. Urushima, T.; Yasui, Y.; Ishikawa, H.; Hayashi, Y., Polymeric Ethyl Glyoxylate in an Asymmetric Aldol Reaction Catalyzed by Diarylprolinol. *Organic letters* **2010,** *12*, 2966-2969.

30. Pirrung, M. C.; Shuey, S. W.; Lever, D. C.; Fallon, L., A convenient procedure for the deprotection of silylated nucleosides and nucleotides using triethylamine trihydrofluoride. *Bioorg. Med. Chem. Lett.* **1994,** *4*, 1345-1346.

31. Sau, S. P.; Fahmi, N. E.; Liao, J.-Y.; Bala, S.; Chaput, J. C., A Scalable Synthesis of α-l-Threose Nucleic Acid Monomers. *The Journal of Organic Chemistry* **2016,** *81* (6), 2302-2307.

32. Yoshikawa, M.; Kato, T.; Takenishi, T., A novel method for phosphorylation of nucleosides to 5′-nucleotides. *Tetrahedron Lett.* **1967,** *8*, 5065-5068.

33. Ludwig, J., A new route to nucleoside 5′-triphosphates. *Acta Biochim. et Biophys. Acad. Sci. Hung.* **1981,** *16*, 131-133.

34. Srivatsan, S. G.; Tor, Y., Synthesis and enzymatic incorporation of a fluorescent pyrimidine ribonucleotide. *Nat Protoc* **2007,** *2* (6), 1547-55.

35. Schlegel, M. K.; Essen, L. O.; Meggers, E., Atomic resolution duplex structure of the simplified nucleic acid GNA. *Chem Commun (Camb)* **2010,** *46* (7), 1094-6.

36. Pinheiro, V. B.; Taylor, A. I.; Cozens, C.; Abramov, M.; Renders, M.; Zhang, S.; Chaput, J. C.; Wengel, J.; Peak-Chew, S.-Y.; McLaughlin, S. H.; Herdewijn, P.; Holliger, P., Synthetic Genetic Polymers Capable of Heredity and Evolution. *Science* **2012,** *336* (6079), 341-344.

37. Yu, H.; Zhang, S.; Dunn, M. R.; Chaput, J. C., An Efficient and Faithful in Vitro Replication System for Threose Nucleic Acid. *Journal of the American Chemical Society* **2013,** *135* (9), 3583-3591.

38. Gardner, A. F.; Jackson, K. M.; Boyle, M. M.; Buss, J. A.; Potapov, V.; Gehring, A. M.; Zatopek, K. M.; Corrêa Jr, I. R.; Ong, J. L.; Jack, W. E., Therminator DNA Polymerase: Modified Nucleotides and Unnatural Substrates. *Frontiers in Molecular Biosciences* **2019,** *6*.

39. Tabor, S.; Richardson, C. C., Effect of manganese ions on the incorporation of dideoxynucleotides by bacteriophage T7 DNA polymerase and Escherichia coli DNA polymerase I. *Proceedings of the National Academy of Sciences* **1989,** *86*, 4076-4080.

40. Wen, J.; Zhang, C.; Chen, X.; Dai, Z.; Li, M.; Ma, W.; Yam, C.; Huang, X.; Xiong, C.; Mei, H., An epimer of threose nucleic acid enhances oligonucleotide exonuclease resistance through end capping. *Commun Chem* **2025,** *8* (1), 144.

41. Kypr, J.; Kejnovska, I.; Renciuk, D.; Vorlickova, M., Circular dichroism and conformational polymorphism of DNA. *Nucleic Acids Res* **2009,** *37* (6), 1713-25.

42. Huang, M.; Giese, T. J.; Lee, T. S.; York, D. M., Improvement of DNA and RNA Sugar Pucker Profiles from Semiempirical Quantum Methods. *J Chem Theory Comput* **2014,** *10* (4), 1538-1545.

43. Mattelaer, C. A.; Mattelaer, H. P.; Rihon, J.; Froeyen, M.; Lescrinier, E., Efficient and Accurate Potential Energy Surfaces of Puckering in Sugar-Modified Nucleosides. *J Chem Theory Comput* **2021,** *17* (6), 3814-3823.

44. Reynders, S.; Rihon, J.; Lescrinier, E., Molecular Modeling on Duplexes with Threose-Based TNA and TPhoNA Reveals Structural Basis for Different Hybridization Affinity toward Complementary Natural Nucleic Acids. *J Chem Theory Comput* **2025,** *21* (5), 2798-2814.

45. Ebert, M. O.; Mang, C.; Krishnamurthy, R.; Eschenmoser, A.; Jaun, B., The Structure of a TNA−TNA complex in solution: NMR study of the octamer duplex derived from α-(L)-threofuranosyl-(3′ -2′)-CGAATTCG. *Journal of the American Chemical Society* **2008,** *130*, 15105-15115.

46. Anosova, I.; Kowal, E. A.; Sisco, N. J.; Sau, S.; Liao, J. y.; Bala, S.; Rozners, E.; Egli, M.; Chaput, J. C.; Van Horn, W. D., Structural Insights into Conformation Differences between DNA/TNA and RNA/TNA Chimeric Duplexes. *ChemBioChem* **2016,** *17* (18), 1705-1708.

47. Tomar, R.; Ghodke, P. P.; Patra, A.; Smyth, E.; Pontarelli, A.; Copp, W.; Guengerich, F. P.; Chaput, J. C.; Wilds, C. J.; Stone, M. P.; Egli, M., DNA Replication across α -l-(3′ -2′)-Threofuranosyl Nucleotides Mediated by Human DNA Polymerase η . *Biochemistry* **2024,** *63* (19), 2425-2439.

48. Castro, C.; Smidansky, E. D.; Arnold, J. J.; Maksimchuk, K. R.; Moustafa, I.; Uchida, A.; Gotte, M.; Konigsberg, W.; Cameron, C. E., Nucleic acid polymerases use a general acid for nucleotidyl transfer. *Nat Struct Mol Biol* **2009,** *16* (2), 212-8.

49. Brown, J. A.; Suo, Z., Unlocking the sugar "steric gate" of DNA polymerases. *Biochemistry* **2011,** *50* (7), 1135-42.

50. Xu, Y.; Reynders, S.; Coosemans, F.; Herdewijn, P.; Groaz, E.; Lescrinier, E., Synthesis of Xylo‐nucleoside H‐Phosphinates and Insights into Their Conformational Preferences Within a Chimeric Duplex. *European Journal of Organic Chemistry* **2025,** *28* (18).

51. Sheppard, T. L.; Breslow, R. C., Selective Binding of RNA, but Not DNA, by Complementary 2‘, 5‘-Linked DNA. *Journal of the American Chemical Society* **1996,** *118*, 9810-9811.

52. Wasner, M.; Arion, D.; Borkow, G.; Noronha, A.; Uddin, A. H.; Parniak, M. A.; Damha, M. J., Physicochemical and Biochemical Properties of 2‘, 5‘-Linked RNA and 2‘,5 ‘-RNA: 3‘, 5‘-RNA “Hybrid” Duplexes. *Biochemistry* **1998,** *37*, 7478-7486.

53. Robinson, H.; Jung, K. E.; Switzer, C.; Wang, A. H. J., DNA with 2'-5'phosphodiester bonds forms a duplex structure in the A-type conformation. *Journal of the American Chemical Society* **1995,** *117*, 837-838.

54. Hajjar, M.; Chim, N.; Liu, C.; Herdewijn, P.; Chaput, J. C., Crystallographic analysis of engineered polymerases synthesizing phosphonomethylthreosyl nucleic acid. *Nucleic Acids Res* **2022,** *50* (17), 9663-9674.